PHILOSOPHICAL TRANSACTIONS A

rsta.royalsocietypublishing.org

Research

Cite this article: García M, Poza J, Santamarta D, Romero-Oraá R, Hornero R. 2018 Continuous wavelet transform in the study of the time-scale properties of intracranial pressure in hydrocephalus. *Phil. Trans. R. Soc. A* **376**: 20170251. http://dx.doi.org/10.1098/rsta.2017.0251

Accepted: 3 April 2018

One contribution of 13 to a theme issue 'Redundancy rules: the continuous wavelet transform comes of age'.

Subject Areas:
biomedical engineering

Keywords:
hydrocephalus, infusion test, intracranial pressure, continuous wavelet transform

Author for correspondence:
María García
e-mail: maria.garcia@tel.uva.es

Electronic supplementary material is available online at https://dx.doi.org/10.6084/m9.figshare.c.4120559.

THE ROYAL SOCIETY PUBLISHING

Continuous wavelet transform in the study of the time-scale properties of intracranial pressure in hydrocephalus

María García[1], Jesús Poza[1,2,3], David Santamarta[4], Roberto Romero-Oraá[1] and Roberto Hornero[1,2,3]

[1]Biomedical Engineering Group (GIB), Department T.S.C.I.T., E.T.S. Ingenieros de Telecomunicación, University of Valladolid, Valladolid, Spain
[2]IMUVA, Instituto de Investigación en Matemáticas, University of Valladolid, Valladolid, Spain
[3]INCYL, Instituto de Neurociencias de Castilla y León, University of Salamanca, Salamanca, Spain
[4]Servicio de Neurocirugía, Complejo Asistencial Universitario de León, León, Spain

MG, 0000-0002-4037-0351

Normal pressure hydrocephalus (NPH) encompasses a heterogeneous group of disorders generally characterized by clinical symptoms, ventriculomegaly and anomalous cerebrospinal fluid (CSF) dynamics. Lumbar infusion tests (ITs) are frequently performed in the preoperatory evaluation of patients who show NPH features. The analysis of intracranial pressure (ICP) signals recorded during ITs could be useful to better understand the pathophysiology underlying NPH and to assist treatment decisions. In this study, 131 ICP signals recorded during ITs were analysed using two continuous wavelet transform (CWT)-derived parameters: Jensen divergence (JD) and spectral flux (SF). These parameters were studied in two frequency bands, associated with different components of the signal: B_1(0.15–0.3 Hz), related to respiratory blood pressure oscillations; and B_2 (0.67–2.5 Hz), related to ICP pulse waves. Statistically significant differences ($p < 1.70 \times 10^{-3}$, Bonferroni-corrected Wilcoxon signed-rank tests) in pairwise comparisons between phases of ITs were found using the mean and standard deviation of JD and SF. These differences were mainly found in B_2, where a lower irregularity and variability, together with less prominent time-frequency fluctuations, were found in

the hypertension phase of ITs. Our results suggest that wavelet analysis could be useful for understanding CSF dynamics in NPH.

This article is part of the theme issue 'Redundancy rules: the continuous wavelet transform comes of age'.

1. Introduction

Adult hydrocephalus comprises a heterogeneous group of disorders occurring in a wide range of ages, chronicity of symptoms and physiological states [1]. Patients with hydrocephalus generally show a triad of clinical symptoms (unsteady gait, urinary incontinence and cognitive impairment), as well as enlarged cerebral ventricles and anomalous cerebrospinal fluid (CSF) dynamics [1–3]. Normal pressure hydrocephalus (NPH) can develop as a consequence of subarachnoid haemorrhage, traumatic brain injury or meningitis [1,4]. However, idiopathic NPH can also appear as a primary condition, without a specific pathological hallmark [4]. Ventricular shunting is a generally accepted treatment of choice [5]. However, the outcome of shunt surgery is not always positive and the management of NPH patients becomes challenging for neurosurgeons [1,6]. In spite of the recent advances, treatment is sometimes based on a reduced knowledge of the underlying pathophysiology [7]. Therefore, the study of intracranial pressure (ICP) and CSF dynamics can provide valuable information for the selection of patients who could benefit from shunt surgery and the management of shunted patients [8].

Lumbar infusion tests (ITs) are regular procedures in the preoperatory evaluation of subjects who show clinical and radiological features of NPH [9]. In ITs, ICP is artificially raised by the injection of fluid in the ventricular or subarachnoidal space. The resulting pressure is subsequently recorded and the resistance to CSF outflow is calculated [9]. The applications of ITs also include shunt function assessment [10], the analysis of metabolic changes in periventricular white matter [11] and the study of the haemodynamic response related to ICP [12].

Traditionally, the analysis of the ICP waveforms relied on the time-averaged mean, provided by most ICP monitoring devices and related to certain pathological patterns [13,14]. This is a simple and widely available measure, but it does not reflect all the information contained in ICP signals and does not clarify NPH pathophysiology [9,13,14]. For this reason, prior research has been devoted to study the ICP waveform using alternative perspectives that take cerebral vascular pathophysiology and cerebral volume compensatory mechanisms into account [14]. In this sense, nonlinear methods, including approximate entropy [15], multiscale entropy [16] and Lempel–Ziv (LZ) complexity [9,17], have been used to analyse ICP signals. Results revealed a loss of complexity induced by intracranial hypertension in children with traumatic brain injury [15,17] and in adults with hydrocephalus [9]. Additionally, reduced complexity seems to be associated with a poor outcome after traumatic brain injury [16]. ICP signal analysis by means of spectral methods has also been addressed in the literature [12,18,19]. Prior research studied the relationship between resistance to CSF outflow and three spectral components of the ICP waveform: pulse, respiratory and slow vasogenic waves [12]. In this regard, the analysis of slow waves has received special interest [18]. In a previous study, ICP recordings obtained during ITs were analysed using two classical spectral parameters: median frequency and relative power [19].

Recent studies have addressed the analysis of ICP recordings using the wavelet transform. This is a suitable methodology due to the non-stationary and multiscale nature of cerebral haemodynamics [20]. Several authors used the wavelet transform to analyse the instantaneous phase difference between arterial blood pressure (ABP) and ICP fluctuations [20]. The wavelet spectrograms have been also analysed as an alternative representation of long-term ICP recordings and ITs [21]. Other studies focused on the calculation of the wavelet transform phase-shift between ABP and ICP signals in patients with traumatic brain injury [22]. The analysis of wavelet coherence to assess cerebral autoregulation in neonates has also received attention [23].

Parameters derived from the wavelet transform of ICP signals, like wavelet entropy (WE) and wavelet turbulence (WT), have been also used to study signal irregularity and variability in ICP recordings obtained during ITs [24]. Alternative time-frequency representations, such as Zhao–Atlas–Marks distribution, have been used to analyse cerebral autoregulation in healthy subjects during hypercapnia [25].

In the present research, our working hypothesis is that NPH elicits a disruption of CSF dynamics that is reflected in instabilities of respiratory- and pulse-related ICP oscillatory components. To study the time-varying properties of ICP signals, we propose computing wavelet-based measures that can accurately reflect the non-stationary and multiscale alterations in ICP associated with NPH. Specifically, we analyse the variability and irregularity patterns of ICP signals using Jensen divergence (JD), and time-frequency fluctuations by means of spectral flux (SF). They are analysed in two frequency bands: B_1, between 0.15 and 0.3 Hz, related to respiratory blood pressure oscillations [26]; and B_2, between 0.67 and 2.5 Hz, related to ICP pulse waves [26]. We attempt to address the following research questions: (i) Can the proposed parameters reflect the dynamical properties of ICP signals recorded during ITs? and (ii) Are the proposed parameters useful to evaluate the influence of respiratory and pulse waves of the ICP waveform in NPH?

2. Material and methods

(a) Subjects

We analysed 131 ICP signals recorded during ITs at the Department of Neurosurgery of the University Hospital of León (Spain). The recordings belonged to patients suffering from hydrocephalus (79 male and 52 female, age 69 ± 14 years, mean $\pm$ s.d.). Brain images (computer tomography or magnetic resonance) revealed ventriculomegaly in 96.18% of patients (Evans index ≥ 0.30). All the participants presented clinical symptoms of NPH: gait and balance disturbances, cognitive deterioration and urinary incontinence [10,27]. Lumbar ITs were performed as a supplementary hydrodynamic study to help in the decision on the surgical management of patients [9,24]. Table 1 summarizes the data of the population under study.

All patients or a close relative gave their informed consent to be included in the study, which was approved by the Ethics Committee at the University Hospital of León (Spain).

(b) Data acquisition protocol

Signals were acquired using a variant of the Katzman and Hussey method [28]. With patients under local anaesthesia and in the lateral recumbent position, two lumbar needles were inserted in the lower lumbar region. The caudal needle was connected to an infusion pump (Lifecare® 5000, Abbott Laboratories) through a three-way stopcock and used to perform infusion. Pressure was measured using the second needle (rostral needle), which was connected to a pressure microtransducer (Codman® MicroSensor™ ICP transducer, Codman & Shurtleff). The analogue output of the microtransducer was connected to an amplifier (ML110 Bridge amplifier), an analogue to digital converter (PowerLab 2/25 Data recording system ML825, ADI Instruments) and a computer, where signals could be visualized and recorded [9,24].

Each ICP recording contained four different phases. Firstly, the opening pressure (P_0) was determined after approximately 5 min of baseline recording. Then, a Ringer solution was infused at a constant rate of 1.5 ml min^{-1}. Infusion stopped when the pressure levels reached a plateau. At this point, the plateau pressure (P_p) was measured. CSF pressure was still recorded after infusion ceased, until it decreased towards the baseline level [9,19]. A qualified neurosurgeon manually selected four artefact-free epochs for signal analysis by visual inspection of each recording [9,19]:

— Epoch 0 (E_0) was representative of the basal phase of the IT. P_0 was measured at this stage.

Table 1. Data recorded from the population under study. IQR, interquartile range.

characteristic	value (median [IQR])
number of subjects (n)	131
age (years)	69 [62–79]
ventricular size (Evans index, E)	0.37 [0.35–0.41]
basal pressure (P_0) (mm Hg)	8.26 [5.72–11.11]
basal amplitude (A_0) (mm Hg)	2.71 [1.57–3.46]
plateau pressure (P_p) (mm Hg)	25.78 [18.12–33.04]
plateau amplitude (A_p) (mm Hg)	10.40 [5.45–13.80]
outflow resistance (R) (mm Hg ml^{-1} min)	11.67 [7.30–15.25]

— Epoch 1 (E_1) corresponded to the early infusion phase, where ICP recordings usually described an ascending slope.
— Epoch 2 (E_2) represented the plateau phase. P_p was obtained in this stage.
— Epoch 3 (E_3) was connected to the recovery phase, where the pressure slowly decreased towards baseline levels.

ICP recordings were acquired with a sampling frequency $f_s = 100$ Hz. All the recordings were processed using a finite impulse response bandpass filter with cut-off frequencies 0.02 and 5 Hz. This frequency range preserved the relevant spectral content of the signals and minimized the presence of the DC component [24].

One of the ICP recordings in our database can be seen in figure 1. The four artefact-free epochs identified by the neurosurgeon have been indicated in this image.

(c) Continuous wavelet transform

The continuous wavelet transform (CWT) is a mathematical tool that can be used to analyse time series with a variable resolution in the time-frequency plane [29]. It has been used in the context of ICP signal analysis due to the non-stationary and multiscale features of cerebral haemodynamics [20,24]. In the CWT, the signal to be analysed, $x(t)$, is decomposed using translated and dilated versions of a function called 'mother wavelet', $\psi(t)$ [29]. For this task, a dilation parameter or scale, s, is considered. Additionally, the location parameter, τ, represents the translation of $\psi(t)$ [30]. The wavelet coefficients, $W(\tau,s)$, quantify the similarity between $x(t)$ and the scaled and translated versions of $\psi(t)$ [29,30]:

$$W(\tau,s) = \frac{1}{\sqrt{s}} \cdot \int_{-\infty}^{\infty} x(t) \cdot \psi^* \left(\frac{t-\tau}{s} \right) \mathrm{d}t. \tag{2.1}$$

Here, * represents the complex conjugate of the wavelet function. A wavelet is a zero-mean and finite-energy function that is localized in both time and frequency [30–32]. Many different waveforms satisfy these conditions and could be used as mother wavelet [29]. In this study, we chose the complex Morlet wavelet. It has the form of a Gaussian-windowed complex sinusoidal waveform with several cycles [33]. The complex Morlet wavelet has been previously used in the analysis of several types of biological signals that show a non-stationary behaviour [20,34–36], including ICP signal analysis [20,24]. It can be defined as [20]

$$\psi(t) = \frac{1}{\sqrt{\pi \Omega_b}} \cdot \exp(j2\pi \Omega_c t) \cdot \exp\left(\frac{-t^2}{\Omega_b} \right), \tag{2.2}$$

where Ω_c is the wavelet centre frequency and Ω_b is the bandwidth parameter. In this study, both parameters were set to 1, in order to obtain a good trade-off between time resolution (Δt) and frequency resolution (Δf) at low frequencies [20].

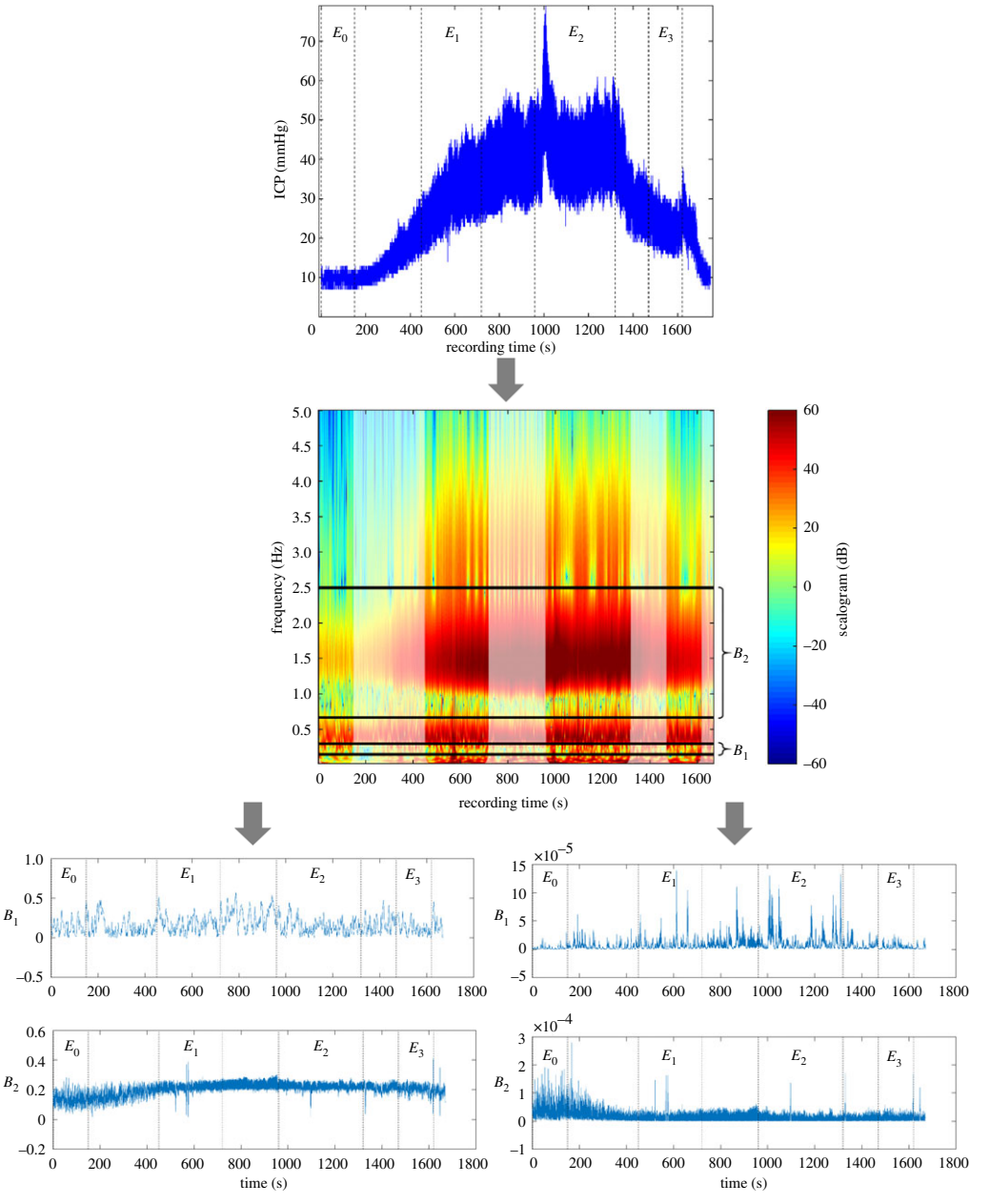

Figure 1. Evolution of the CSF pressure during the IT for a patient diagnosed with normal pressure hydrocephalus (top panel). The four artefact-free epochs selected by a neurosurgeon have been indicated (E_0: Epoch 0, E_1: Epoch 1, E_2: Epoch 2, E_3: Epoch 3). Scalogram obtained for the ICP recording (middle panel). The transparency outline delineates the limits of the cone of influence (COI), where border effects can be ignored. The black horizontal lines indicate the limits of frequency bands B_1 (0.15–0.3 Hz) and B_2 (0.67–2.5 Hz). Evolution of JD along time for frequency bands B_1 and B_2 (bottom left panel). Evolution of SF along time for frequency bands B_1 and B_2 (bottom right panel). (Online version in colour.)

Actually, the relationship between Δt and Δf is important in wavelet analysis. According to the Heisenberg uncertainty principle, it is not possible to achieve arbitrarily good resolution in time and frequency simultaneously [31]. The CWT provides good Δt at high frequencies and good Δf at low frequencies [29,30]. To take this issue into account, we defined a Heisenberg box in the calculation of the CWT. It is a rectangle centred at each point in the time-frequency plane, whose

width and height depend on the time and frequency resolution [30,32]. It should also be noticed that the four artefact-free epochs analysed are finite short-time signal segments. This means that CWT calculation would be affected by edge effects at the beginning and end of each epoch [31]. To take this problem into account, a cone of influence (COI) was established for each of the four artefact-free epochs based on the Heisenberg box approach. The COI delimitates the region in the time-frequency plane in which edge effects can be ignored [31]. The area of the Heisenberg box was chosen to be $2\Delta t \times 2\Delta f$ [34]. In figure 1, the scalogram and COIs corresponding to the artefact-free epochs of the example ICP signal are depicted.

The ICP recordings in our database were analysed in two frequency bands. B_1 encompasses the frequency range between 0.15 and 0.3 Hz (9–18 cycles per minute) and is related to respiratory blood pressure oscillations [26]. B_2 corresponds to frequencies between 0.67 and 2.5 Hz (40–150 cycles per minute) and is related to ICP pulse waves [26]. Only those CWT coefficients whose associated Heisenberg boxes were completely included in the COI for the scales associated with frequencies in B_1 and B_2 were taken into account [34].

(d) Jensen divergence

Irregularity of ICP signals during ITs has been previously analysed using measures of entropy obtained from a time-scale representation of the signal trough of the CWT [24]. In this case, the classical measure of the Shannon entropy is called the WE [24]. Measures of entropy are useful in quantifying the disorder of a system. However, they do not describe the underlying system [37]. In this regard, information theory introduces the concept of disequilibrium [37]. More specifically, disequilibrium provides a quantification of the distance between a probability density function (PDF), P, and the PDF that represents the equilibrium, P_e [37,38]:

$$Q[P] = Q_0 \cdot D[P, P_e], \tag{2.3}$$

where $D[\cdot]$ represents a measure of distance and Q_0 is a normalization constant. Although many distance measures can be applied, it is also possible to use a divergence metric [38]. In this study, we used JD, which is a symmetric and smoothed version of the well-known Kullback–Leibler divergence [39]. One of the advantages of JD over other divergence measures is that the probability distributions involved do not need to meet the condition of absolute continuity [39]. JD can be expressed from the WE as [38]

$$\mathrm{JD}[P_1, P_2] = \mathrm{WE}\left[\frac{P_1 + P_2}{2}\right] - \mathrm{WE}\left[\frac{P_1}{2}\right] - \mathrm{WE}\left[\frac{P_2}{2}\right]. \tag{2.4}$$

JD quantifies the difference between two PDFs, P_1 and P_2. In order to be a disequilibrium measure, P_1 is replaced by the PDF of the system under consideration and P_2 by the PDF representing the equilibrium, i.e. P_e. In this study, P_e is represented by a uniform PDF. In the same way, the normalized wavelet scalogram, obtained from $W(\tau,s)$, was used to represent the PDF of the system under consideration [37]:

$$W_n(\tau,s) = \frac{|W(\tau,s)|^2}{\sum_s |W(\tau,s)|^2}, \tau = 1, \ldots, N_T, s \in S_{B_i} (i = 1,2), \tag{2.5}$$

where S_{B_i} represents the subset of scales corresponding to frequencies in B_i ($i = 1,2$).

JD was calculated at each time point in the scales corresponding to frequency bands B_1 and B_2. Therefore, we obtained the temporal evolution of this parameter for each frequency band (see figure 1, bottom left panel). The mean ($\langle \mathrm{JD} \rangle$) and the standard deviation (SD[JD]) were subsequently calculated from the time series formed by the temporal evolution of JD in frequency bands B_1 and B_2. $\langle \mathrm{JD} \rangle$ summarizes the average irregularity throughout time, while SD[JD] describes the variability of the JD around the mean value. An average value of $\langle \mathrm{JD} \rangle$ and SD[JD] was obtained for each artefact-free epoch and frequency band. We will denote by $\langle \mathrm{JD}_{B_i}^{E_j} \rangle$ the average value of JD in epoch E_j ($j = 0,1,2,3$) and band B_i ($i = 1,2$). Similarly, $\mathrm{SD}[\mathrm{JD}_{B_i}^{E_j}]$ denotes

the value of SD[JD] in epoch E_j ($j=0,1,2,3$) and band B_i ($i=1,2$). The evolution of JD along time for the two frequency bands of interest has also been depicted in figure 1.

(e) Spectral flux

As previously mentioned, irregularity patterns of ICP signals have been analysed in other studies. Although they provide an interesting approach to understanding ICP properties, they are not able to assess ICP instabilities in NPH. Therefore, new approaches are needed. We introduced SF as a novel time-varying parameter, useful to quantify spatio-temporal oscillations in neural signals [40]. In this study, SF was used to assess temporal fluctuations in ICP signals. It is defined as the statistical distance between consecutive scalograms along the duration of the signal [40]:

$$\mathrm{SF}(\tau) = D_\alpha[\mathrm{WS}(\tau, s), \mathrm{WS}(\tau + T_\mathrm{s}, s)], \tag{2.6}$$

where T_s is the sampling period ($T_\mathrm{s}=1/f_\mathrm{s}$) and D_α represents a statistical distance. In this sense, SF can be considered a dynamical measure that quantifies the spectral fluctuations that occur within the signal along time. As in the case of JD, different distance measures could be used, but it is also possible to consider a divergence metric [38]. In order to be consistent with the previous parameter, JD was employed in the calculation of SF. However, in this case, the divergence provides a measure of the differences that occur *within* the signal at different time points. Conversely, in the previous parameter (JD) the distance measure was useful to quantify the differences between the signal and the PDF that represents the equilibrium.

We obtained the temporal evolution of SF in frequency bands B_1 and B_2 by applying (2.6) in the scales corresponding to each frequency band. The mean ($\langle\mathrm{SF}\rangle$) and the standard deviation (SD[SF]) were subsequently calculated from this time series. $\langle\mathrm{SF}\rangle$ quantifies the average value of the dynamical spectral fluctuations within the signal, while SD[SF] describes the variability of these spectral fluctuations around the mean value. An average value of SF and SD[SF] was obtained for each artefact-free epoch and frequency band. We will denote by $\langle\mathrm{SF}_{B_i}^{E_j}\rangle$ the average value of SF in epoch E_j ($j=0,1,2,3$) and band B_i ($i=1,2$). Similarly, $\mathrm{SD}[\mathrm{SF}_{B_i}^{E_j}]$ denotes the value of SD[SF] in epoch E_j ($j=0,1,2,3$) and band B_i ($i=1,2$). The evolution of SF along time can be seen in figure 1 for B_1 and B_2.

(f) Statistical analysis

Data distribution was initially studied by means of an exploratory analysis. The Kolmogorov–Smirnov with Lilliefors significance correction and the Shapiro–Wilk tests were used to determine the normality of JD and SF in the four artefact-free epochs. The results showed that our data did not meet parametric test assumptions. Therefore, the existence of statistically significant interactions ($\alpha=0.01$) among epochs of the IT was assessed using the non-parametric Friedman test [41]. Post hoc analyses were performed when statistically significant interactions were found. For this task, the Wilcoxon signed-rank test with Bonferroni-correction to account for multiple comparisons ($\alpha=0.01/6=1.7\times10^{-3}$) was used [41].

3. Results

Table 2 summarizes the median and interquartile range (IQR) of CSF pressure and epoch duration. These values were averaged over the 131 subjects in our database.

(a) Jensen divergence results

The non-parametric Friedman test showed significant interactions among phases of the IT using $\langle\mathrm{JD}_{B_1}\rangle$ ($\chi^2(3)=17.75, p=4.96\times10^{-4}$), $\langle\mathrm{JD}_{B_2}\rangle$ ($\chi^2(3)=83.18, p=6.38\times10^{-18}$) and $\mathrm{SD}[\mathrm{JD}_{B_2}]$ ($\chi^2(3)=139.46, p=4.94\times10^{-30}$). The Wilcoxon signed-rank test with Bonferroni-correction was used to perform post hoc analyses in order to evaluate these interactions. Statistically significant

Table 2. Median [interquartile range, IQR] values of the epoch length and CSF pressure.

	Epoch 0	Epoch 1	Epoch 2	Epoch 3
length (s)	150 [120–180]	300 [240–300]	429 [308–540]	160 [120–180]
CSF pressure (mm Hg)	7.72 [5.72–11.11]	16.13 [12.07–20.79]	24.91 [18.12–33.04]	15.26 [11.69–19.80]

differences were found between several pairwise comparisons of artefact-free epochs of ITs, as summarized in table 3.

Additionally, the evolution of $\langle JD_{B_i}^{E_j} \rangle$ and $SD[JD_{B_i}^{E_j}]$ ($j = 0,1,2,3$ and $i = 1,2$) along the IT was analysed (figure 2). $\langle JD_{B_1} \rangle$ values were higher in E_0, slightly decreased during infusion reaching the lowest values in E_2 and then increased again in E_3. Regarding $SD[JD_{B_1}]$, values were very similar in all epochs of the IT. The results in B_2 followed a different trend. The minimum $\langle JD_{B_2} \rangle$ values were found in the basal phase and then increased during infusion until the plateau phase. $\langle JD_{B_2} \rangle$ slightly decreased again in the recovery phase. Regarding $SD[JD_{B_2}]$, the highest values corresponded to the basal phase. Then $SD[JD_{B_2}]$ decreased during infusion, reaching the lowest levels in the plateau phase. Finally, $SD[JD_{B_2}]$ increased again in E_3.

(b) Spectral flux results

The results of the Friedman test revealed significant interactions among phases of the IT using $\langle SF_{B_1} \rangle$ ($\chi^2(3) = 40.99, p = 6.58 \times 10^{-9}$), $SD[SF_{B_1}]$ ($\chi^2(3) = 42.60, p = 2.99 \times 10^{-9}$), $\langle SF_{B_2} \rangle$ ($\chi^2(3) = 79.88, p = 3.26 \times 10^{-17}$) and $SD[SF_{B_2}]$ ($\chi^2(3) = 92.03, p = 8.03 \times 10^{-20}$). Post hoc analyses were subsequently performed to analyse these interactions. Statistically significant differences were detected in pairwise comparisons between different phases of ITs in frequency bands B_1 and B_2, as shown in table 3.

The temporal evolution of $\langle SF_{B_i}^{E_j} \rangle$ and $SD[SF_{B_i}^{E_j}]$ ($j = 0,1,2,3$ and $i = 1,2$) is depicted in figure 3. The tendency was very similar using $\langle SF_{B_1} \rangle$ and $SD[SF_{B_1}]$: the lowest values were found in the basal phase, then increased during infusion until the plateau phase, slightly decreasing again in the recovery phase. In the case of band B_2, the values of $\langle SF_{B_2} \rangle$ and $SD[SF_{B_2}]$ were higher in E_0, decreased during infusion to reach the lowest values in E_2 and then slightly increased again in E_3.

4. Discussion and conclusion

(a) Dynamical properties of intracranial pressure signals

Regarding the first research question, results for JD in band B_1 showed non-significant differences between phases of the IT using $\langle JD_{B_1} \rangle$ and $SD[JD_{B_1}]$. In the case of band B_2, we found statistically significant differences between the basal phase and the remaining phases of the ITs using $\langle JD_{B_2} \rangle$ and $SD[JD_{B_2}]$. It should be noted that our results showed a significant increase in $\langle JD_{B_2}^{E_2} \rangle$ with respect to $\langle JD_{B_2}^{E_0} \rangle$. This indicates that, during the state of intracranial hypertension, the average irregularity throughout time decreases when compared with the resting state. These changes were only found in B_2, suggesting that this irregularity decrease is mainly associated with the pulse waves [12]. This result is consistent with findings obtained in previous studies, where an irregularity loss in E_2 with respect to E_0 was found using WE and WT [24]. However, in this study, irregularity was measured in terms of disequilibrium and using divergence as a distance measure. A decrease in complexity during episodes of intracranial hypertension has also been reported [9,17]. A decrease in LZ complexity in the plateau phase of ITs with respect to the basal phase was found in adults [9]. Reduced complexity has also been found in paediatric patients suffering from traumatic brain injury and intracranial hypertension [17]. Certainly, complexity and irregularity are complementary measures to quantify the degree of disorder in a system. It should also be stressed that a significant decrease in $SD[JD_{B_2}^{E_2}]$ with respect to $SD[JD_{B_2}^{E_0}]$ was found.

Table 3. Z statistics and p-values associated with the Wilcoxon signed-rank tests. The significant values ($p < 1.70 \times 10^{-3}$, Bonferroni-corrected) are in italic. E_0, Epoch 0; E_1, Epoch 1; E_2, Epoch 2; E_3, Epoch 3; $\langle \mathrm{JD}_{B_1} \rangle$, mean Jensen's divergence in band B_1; $\mathrm{SD}[\mathrm{JD}_{B_1}]$, standard deviation of the Jensen's divergence in band B_1; $\langle \mathrm{JD}_{B_2} \rangle$, mean Jensen's divergence in band B_2; $\mathrm{SD}[\mathrm{JD}_{B_2}]$, standard deviation of the Jensen's divergence in band B_2; $\langle \mathrm{SF}_{B_1} \rangle$, mean spectral flux in band B_1; $\mathrm{SD}[\mathrm{SF}_{B_1}]$, standard deviation of the spectral flux in band B_1; $\langle \mathrm{SF}_{B_2} \rangle$, mean spectral flux in band B_2; $\mathrm{SD}[\mathrm{SF}_{B_2}]$, standard deviation of the spectral flux in band B_2.

	E_0 versus E_1		E_0 versus E_2		E_0 versus E_3		E_1 versus E_2		E_1 versus E_3		E_2 versus E_3	
	Z	p-value	Z	p-value	Z	p-value	Z	p-value	Z	p-value	Z	p-value
$\langle \mathrm{JD}_{B_1} \rangle$	−1.68	9.27×10^{-2}	−3.11	1.90×10^{-3}	−2.38	1.74×10^{-2}	−2.18	1.89×10^{-2}	−2.44	1.46×10^{-2}	−0.40	0.69
$\mathrm{SD}[\mathrm{JD}_{B_1}]$	−1.22	0.22	−0.21	0.83	−0.94	0.35	−0.90	0.37	−0.45	0.65	−1.30	0.19
$\langle \mathrm{JD}_{B_2} \rangle$	−6.89	*5.69×10^{-12}*	−7.39	*1.44×10^{-13}*	−6.60	*4.18×10^{-11}*	−3.03	2.50×10^{-3}	−0.05	0.96	−3.40	*6.80×10^{-4}*
$\mathrm{SD}[\mathrm{JD}_{B_2}]$	−7.11	*1.20×10^{-12}*	−8.21	*2.16×10^{-16}*	−8.02	*1.02×10^{-15}*	−6.13	*8.59×10^{-10}*	−3.88	*1.04×10^{-4}*	−2.93	3.40×10^{-3}
$\langle \mathrm{SF}_{B_1} \rangle$	−3.31	*9.32×10^{-4}*	−4.21	*2.52×10^{-5}*	−2.21	2.74×10^{-2}	−3.86	*1.13×10^{-4}*	−0.32	0.75	−2.94	3.30×10^{-3}
$\mathrm{SD}[\mathrm{SF}_{B_1}]$	−2.90	3.70×10^{-3}	−4.56	*5.23×10^{-6}*	−2.39	1.69×10^{-2}	−3.84	*1.24×10^{-4}*	−0.005	0.99	−3.39	*6.91×10^{-4}*
$\langle \mathrm{SF}_{B_2} \rangle$	−6.47	*1.00×10^{-10}*	−7.25	*4.31×10^{-13}*	−6.97	*3.12×10^{-12}*	−2.95	3.20×10^{-3}	−0.94	0.35	−2.16	3.10×10^{-2}
$\mathrm{SD}[\mathrm{SF}_{B_2}]$	−7.19	*6.57×10^{-13}*	−8.13	*4.46×10^{-16}*	−7.81	*5.59×10^{-15}*	−3.31	*9.32×10^{-4}*	−1.36	0.17	−2.18	2.96×10^{-2}

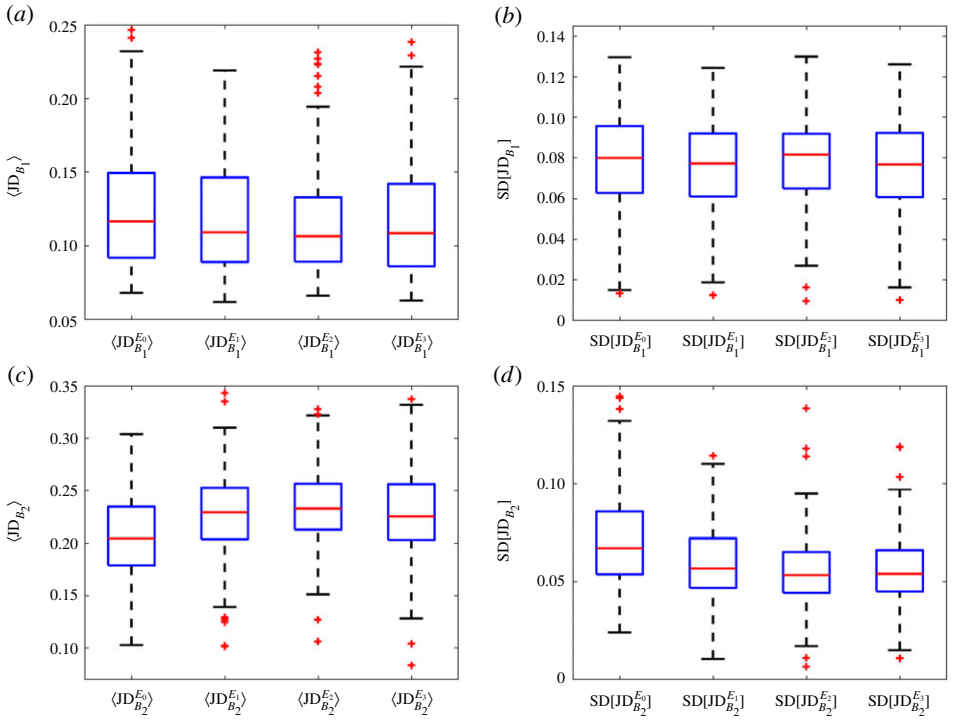

Figure 2. Boxplots showing the distribution of $\langle JD \rangle$ and SD[JD] for frequency bands B_1 and B_2 in the four artefact-free epochs. (*a*) $\langle JD_{B_1} \rangle$, (*b*) $SD[JD_{B_1}]$, (*c*) $\langle JD_{B_2} \rangle$ and (*d*) $SD[JD_{B_2}]$. (Online version in colour.)

This result can be associated with a loss of variability in the plateau phase when compared with the basal phase.

Regarding SF, we found statistically significant differences between phases of the IT in bands B_1 and B_2. Results in table 3 indicate that a significant increase was found in $\langle SF_{B_1}^{E_2} \rangle$ with respect to $\langle SF_{B_1}^{E_0} \rangle$ and in $SD[SF_{B_1}^{E_2}]$ with respect to $SD[SF_{B_1}^{E_0}]$. The tendency found in $\langle SF_{B_1} \rangle$ revealed that the dynamical fluctuations within the signal are more prominent in E_2 with respect to E_0. The variation of these fluctuations around the mean value also increased during the early infusion and plateau phases of the IT. However, the tendency in B_2 was different. Specifically, we found statistically significant differences in $\langle SF_{B_2}^{E_2} \rangle$ with respect to $\langle SF_{B_2}^{E_0} \rangle$. Our results suggests that the signal is less fluctuant in the hypertension state than in the resting state. These findings for band B_2 were concordant with the results obtained with JD, because the irregularity loss during infusion previously found is coherent with a less fluctuant signal in the plateau phase. This result is also coherent with our previous study, where we used WE and WT to measure irregularity [24]. However, SF differs from WE and WT, because it is a parameter focused on the quantification of the signal dynamical fluctuations. As formerly stated, similar results were found using complexity measures in previous studies [9,17]. Regarding $SD[SF_{B_2}]$, we also found a significant decrease in $SD[SF_{B_2}^{E_2}]$ with respect to $SD[SF_{B_2}^{E_0}]$. These results suggest that intracranial hypertension due to volume loading produces a decrease in the variability of the spectral fluctuations around the mean value in band B_2. This variability loss in the plateau phase with respect to the basal phase was also found using $SD[JD_{B_2}]$. A similar result was found in previous studies on ITs, where a decrease in data dispersion, measured in terms of the standard deviation of LZ values, was reported [9]. However, contradictory data can be found in the literature. In [27], an increased variability during intracranial hypertension, measured in terms of data dispersion using central tendency measure, was obtained. Our results using $SD[SF_{B_1}]$ also

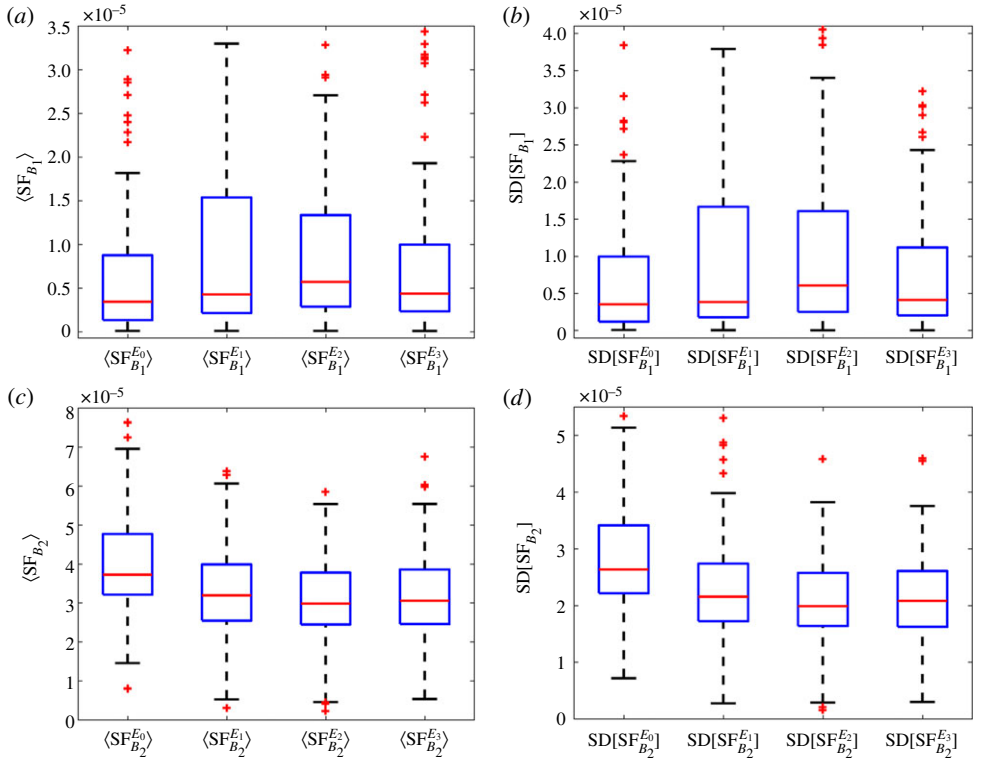

Figure 3. Boxplots showing the distribution of ⟨SF⟩ and SD[SF] for frequency bands B_1 and B_2 in the four artefact-free epochs. (*a*) $\langle SF_{B_1} \rangle$, (*b*) $SD[SF_{B_1}]$, (*c*) $\langle SF_{B_2} \rangle$ and (*d*) $SD[SF_{B_2}]$. (Online version in colour.)

showed an increased variability in the plateau phase with respect to the basal phase. However, it is difficult to clearly assess the relationship between our results and those reported in the literature because variability is quantified differently and the frequency components of the ICP waveform were not studied separately.

In summary, we characterized the irregularity, variability and dynamical fluctuation of ICP signals during ITs using JD and SF. JD provides an alternative measure of the disorder of a system through the concept of divergence, whereas SF represents a novel time-varying parameter that quantifies the fluctuations that occur within the signal at different time points. Our findings support the results in previous studies on ICP signals recorded during ITs, where decreased irregularity and variability in B_2 during the plateau phase were also found. Furthermore, the dynamical nature of the fluctuations in ICP signals was characterized through SF. To the best of our knowledge, this analysis has not been previously addressed. We found different tendencies in B_1 and B_2, which may be linked to the variability of the signal in both frequency bands. Our results support the notion that the individual study of the different components of the ICP waveform is useful in understanding the different physiological elements of NPH.

(b) Respiratory and pulse-related abnormalities in NPH

The second research question was related to the influence of the components of the ICP waveform in NPH physiology. It has been shown that the oscillatory processes that occur in the brain are not only relevant to the function of the central nervous system. They also interact with other physiological oscillations, including the cardiovascular and respiratory systems [42,43]. In this sense, the differences in the average irregularity, dynamical fluctuations and variability found in E_2 with respect to E_0 could be related to various effects. In the first place, NPH has been

associated with a reduced intracranial compliance [44]. Vascular compliance is defined as the rate of change in the vascular volume with respect to pressure changes that occur during the cardiac cycle [44,45]. ICP oscillates as a result of cardiac-driven variations in ABP [46]. The blood volume entering the brain changes within the cardiac cycle, resulting in a net inflow during systole and net outflow during diastole [44]. In order to maintain a stable ICP, these blood volume changes during the cardiac cycle must be compensated by CSF, leading to ABP-driven pulsations in CSF pressure [44]. When compliance is reduced, as in NPH [46], CSF cannot accommodate the volume changes during the cardiac cycle. Besides, it has been suggested that volume load during ITs may also have a relevant impact in brain and blood vessels compliance. This issue leads to an exhausted compensatory reserve in the plateau phase of ITs, independently of the pathogenesis of hydrocephalus [8,47]. In this study, we found a decrease in irregularity and variability of the ICP waveform in the plateau phase with respect to the basal phase. These changes were mainly observed in band B_2, related to pulse waves [26]. Moreover, SF revealed that dynamical fluctuations of the ICP signal in band B_2 were less prominent in the plateau phase than in the basal phase. These results may be a consequence of alterations in the ICP waveform associated with reduced brain compliance in NPH or with hypertension induced by ITs.

The transmission of arterial pulsations through the CSF is also related to the *windkessel* effect [48]. Arterial pulsations suffer a progressive decrease, mostly through the CSF, in order to reach the capillaries of the brain as a non-pulsatile continuous flow [48,49]. Several authors have shown that this occurs as a consequence of a close coupling between CSF oscillations and arterial pulsations, which leads to a resonance state [49]. However, alterations such as NPH cause a disruption of the *windkessel* effect [48,49]. Consequently, the arterial pulse pressure transmitted to the brain capillary bed would be stronger [48]. Our results showed that intracranial hypertension induced by ITs influences the properties of the ABP component of the ICP waveform (band B_2) and may be associated with a disruption of the *windkessel* effect activated by infusion.

Finally, it has been suggested that the moderate rise in ICP during ITs may result in a reversible pressure-driven systemic response [50]. This includes an elevation in ABP and heart rate variability, as well as a decrease in cerebral perfusion pressure and blood flow velocity (FV) [50]. This relationship between pressure and the response of the cardiovascular system is consistent with the presence of an intracranial baroreflex triggered by ITs [50,51]. Our results in band B_2 could be indicative of this adaptive haemodynamic response, which may result in an early Cushing effect that affects ABP [50].

The statistically significant differences between phases of the IT were mainly found in B_2, which leads us to hypothesize that intracranial hypertension induced by ITs mainly affects the pulse component of the ICP waveform. However, some statistically significant differences were also observed in band B_1, related to the respiratory component of the ICP signals. Previous research also reported a relationship between pressure changes and the respiratory component of the ICP waveform [26,52]. It has been shown that, under reduced pressure–volume compliance conditions, ventilatory alternations in cerebral FV are reduced [26,52], while ICP appears to be unaffected [26]. Our results using $\langle \mathrm{SF}_{B_1} \rangle$ indicate that the dynamical fluctuations in the spectral content are more prominent in the plateau phase than in the resting state. In addition, the results obtained for $\mathrm{SD}[\mathrm{SF}_{B_1}]$ suggest that there is a significantly higher variability in the spectral content of band B_1 when CSF pressure reaches the range of intracranial hypertension. However, results were not as significant as in B_2. The methodology used in previous studies was very different from ours, and included experimental models [52] and evoked respiratory waves [26]. This may be the reason why our results show a weaker link between ICP and respiratory waves.

(c) Limitations of the study and future research lines

Certain limitations of the study should be mentioned. Firstly, it should be noted that the ICP waveform contains a third component: slow waves (0.0055–0.05 Hz) [12]. In this study, this frequency range could not be analysed due to the constraints imposed by the duration of the

artefact-free epochs in our database and the frequency resolution associated with the complex Morlet wavelet. Very low frequencies have been previously analysed for brain pressure signals using the wavelet transform, for example in the context of near-infrared spectroscopy signals [53], analysis of ABP and ICP in traumatic brain injury [22] or blood FV and ABP investigation [36]. The analysis of this frequency range was possible because the recording time was longer. Nonetheless, to the best of our knowledge, the COI was only considered in some of these studies [22,23]. It should be mentioned that although slow waves are usually analysed in longer ICP signals, their study may be clinically relevant, because there is evidence that a frequent occurrence of these waves could be related to a positive response to shunting [54]. Further investigations should be performed to assess whether very low frequency components could provide additional information about the mechanisms of cerebral autoregulation. Another important issue concerns the population under study. Although all the patients showed clinical and radiological features of NPH, the mechanisms leading to hydrocephalus were diverse. We believe that patient heterogeneity should not be regarded as an important drawback because this study is focused on the wavelet characterization of ICP signals.

Future efforts will be aimed at studying new wavelet parameters in order to determine whether they can reveal differences between phases of ITs. We will also try to combine wavelet and nonlinear parameters in order to obtain complementary information that may help physicians gain insight into the pathophysiology of NPH. Finally, the potential clinical applications of our results need to be further explored. In this sense, it would be desirable to assess the utility of the proposed wavelet analysis in the prediction of patient response to shunting and in the distinction between NPH and other pathologies with similar clinical signs.

In conclusion, wavelet parameters like JD and SF revealed changes in the signal time-scale representation during ITs. Our results showed a lower irregularity and variability, as well as less prominent spectral fluctuations in the plateau phase with respect to the basal phase in band B_2. We also found statistically significant differences between E_2 and E_0 for band B_1 using SF.

Data accessibility. The datasets supporting this article have been uploaded as part of the electronic supplementary material.

Authors' contributions. M.G.: conception and design of the work, software development, data analysis, interpretation of data, drafting of the manuscript and final approval of the version to be published; J.P.: conception and design of the work, software development, comprehensive revision of the work and final approval of the version to be published; D.S.: acquisition of data, interpretation of data, comprehensive revision of the work and final approval of the version to be published; R.R-O.: interpretation of data, comprehensive revision of the work and final approval of the version to be published; R.H.: interpretation of data, comprehensive revision of the work and final approval of the version to be published.

Competing interests. We have no competing interests.

Funding. This research was supported by 'Ministerio de Economía y Competitividad' and 'European Regional Development Fund' (FEDER) under project TEC2014-53196-R and DPI2017-84280-R, by the 'European Commission' and FEDER under project 'Análisis y correlación entre el genoma completo y la actividad cerebral para la ayuda en el diagnóstico de la enfermedad de Alzheimer' (Cooperation Programme Interreg V-A Spain-Portugal POCTEP 2014-2020), and by 'Consejería de Educación de la Junta de Castilla y León' and FEDER under project VA037U16.

References

1. Bergsneider M, Miller C. 2008 Surgical management of adult hydrocephalus. *Surgery* **62**, 643–660. (doi:10.1227/01.NEU.0000296954.22901.C6)
2. Weerakkody RA, Czosnyka M, Schuhmann MU, Schmidt EA, Keong N, Santarius T, Pickard JD, Czosnyka ZH. 2011 Clinical assessment of cerebrospinal fluid dynamics in hydrocephalus. Guide to interpretation based on observational study. *Acta Neurol. Scand.* **124**, 85–98. (doi:10.1111/j.1600-0404.2010.01467.x)
3. Eide PK, Sorteberg W. 2016 Outcome of surgery for idiopathic normal pressure hydrocephalus: role of preoperative static and pulsatile intracranial pressure. *World Neurosurg.* **86**, 186–193.e1. (doi:10.1016/j.wneu.2015.09.067)

4. Serulle Y *et al.* 2014 Differentiating shunt-responsive normal pressure hydrocephalus from Alzheimer disease and normal aging: pilot study using automated MRI brain tissue segmentation. *J. Neurol.* **261**, 1994–2002. (doi:10.1007/s00415-014-7454-0)
5. Chari A, Czosnyka M, Richards HK, Pickard JD, Czosnyka ZH. 2014 Hydrocephalus shunt technology: 20 years of experience from the Cambridge Shunt Evaluation Laboratory. *J. Neurosurg.* **120**, 697–707. (doi:10.3171/2013.11.JNS121895)
6. Lenfeldt N, Larsson A, Nyberg L, Andersson M, Birgander R, Eklund A, Malm J. 2008 Idiopathic normal pressure hydrocephalus: increased supplementary motor activity accounts for improvement after CSF drainage. *Brain* **131**, 2904–2912. (doi:10.1093/brain/awn232)
7. Eide PK. 2011 Cardiac output in idiopathic normal pressure hydrocephalus: association with arterial blood pressure and intracranial pressure wave amplitudes and outcome of shunt surgery. *Fluids Barriers CNS* **8**, 11. (doi:10.1186/2045-8118-8-11)
8. Czosnyka M, Czosnyka ZH, Momjian S, Pickard JD. 2004 Cerebrospinal fluid dynamics. *Physiol. Meas.* **25**, R51–R76. (doi:10.1088/0967-3334/25/5/R01)
9. Santamarta D, Hornero R, Abásolo D, Martínez-Madrigal M, Fernández J, García-Cosamalón J. 2010 Complexity analysis of the cerebrospinal fluid pulse waveform during infusion studies. *Child's Nerv. Syst.* **26**, 1683–1689. (doi:10.1007/s00381-010-1244-5)
10. Eklund A, Smielewski P, Chambers I, Alperin N, Malm J, Czosnyka M, Marmarou A. 2007 Assessment of cerebrospinal fluid outflow resistance. *Med. Biol. Eng. Comput.* **45**, 719–735. (doi:10.1007/s11517-007-0199-5)
11. Agren-Wilsson A, Eklund A, Koskinen L-OD, Bergenheim AT, Malm J. 2005 Brain energy metabolism and intracranial pressure in idiopathic adult hydrocephalus syndrome. *J. Neurol. Neurosurg. Psychiatry* **76**, 1088–1093. (doi:10.1136/jnnp.2004.042838)
12. Momjian S, Czosnyka ZH, Czosnyka M, Pickard JD. 2004 Link between vasogenic waves of intracranial pressure and cerebrospinal fluid outflow resistance in normal pressure hydrocephalus. *Br. J. Neurosurg.* **18**, 56–61. (doi:10.1080/02688690410001660481)
13. Czosnyka M, Pickard JD. 2004 Monitoring and interpretation of intracranial pressure. *J. Neurol. Neurosurg. Psychiatry* **75**, 813–821. (doi:10.1136/jnnp.2003.033126)
14. Hu X, Xu P, Scalzo F, Vespa P, Bergsneider M. 2009 Morphological clustering and analysis of continuous intracranial pressure. *IEEE Trans. Biomed. Eng.* **56**, 696–705. (doi:10.1109/TBME.2008.2008636)
15. Hornero R, Aboy M, Abásolo D, McNames J, Goldstein B. 2005 Interpretation of approximate entropy: analysis of intracranial pressure approximate entropy during acute intracranial hypertension. *IEEE Trans. Biomed. Eng.* **52**, 1671–1680. (doi:10.1109/TBME.2005.855722)
16. Lu C-W, Czosnyka M, Shieh J-S, Smielewska A, Pickard JD, Smielewski P. 2012 Complexity of intracranial pressure correlates with outcome after traumatic brain injury. *Brain* **135**, 2399–2408. (doi:10.1093/brain/aws155)
17. Hornero R, Aboy M, Abásolo D. 2007 Analysis of intracranial pressure during acute intracranial hypertension using Lempel-Ziv complexity: further evidence. *Med. Biol. Eng. Comput.* **45**, 617–620. (doi:10.1007/s11517-007-0194-x)
18. Lemaire JJ, Boire JY, Chazal J, Irthum B. 1994 A computer software for frequential analysis of slow intracranial pressure waves. *Comput. Methods Programs Biomed.* **42**, 1–14. (doi:10.1016/0169-2607(94)90133-3)
19. García M, Poza J, Santamarta D, Abásolo D, Barrio P, Hornero R. 2013 Spectral analysis of intracranial pressure signals recorded during infusion studies in patients with hydrocephalus. *Med. Eng. Phys.* **35**, 1490–1498. (doi:10.1016/j.medengphy.2013.04.002)
20. Latka M, Kolodziej W, Turalska M, Latka D, Zub W, West BJ. 2007 Wavelet assessment of cerebrospinal compensatory reserve and cerebrovascular reactivity. *Physiol. Meas.* **28**, 465–479. (doi:10.1088/0967-3334/28/5/002)
21. Heissler HE, König K, Krauss JK, Rickels E. 2012 Stationarity in neuromonitoring data. *Acta Neurochir. Suppl.* **114**, 93–95. (doi:10.1007/978-3-7091-0956-4_16)
22. Liu X *et al.* 2017 Cerebrovascular pressure reactivity monitoring using wavelet analysis in traumatic brain injury patients: a retrospective study. *PLoS Med.* **14**, e1002348. (doi:10.1371/journal.pmed.1002348)
23. Tian F, Tarumi T, Liu H, Zhang R, Chalak L. 2016 Wavelet coherence analysis of dynamic cerebral autoregulation in neonatal hypoxic–ischemic encephalopathy. *NeuroImage Clin.* **11**, 124–132. (doi:10.1016/j.nicl.2016.01.020)

24. García M, Poza J, Bachiller A, Santamarta D, Hornero R. 2016 Effect of infusion tests on the dynamical properties of intracranial pressure in hydrocephalus. *Comput. Methods Programs Biomed.* **134**, 225–235. (doi:10.1016/j.cmpb.2016.06.007)
25. Placek MM, Wachel P, Iskander DR, Smielewski P, Uryga A, Mielczarek A, Szczepański TA, Kasprowicz M. 2017 Applying time-frequency analysis to assess cerebral autoregulation during hypercapnia. *PLoS ONE* **12**, e0181851. (doi:10.1371/journal.pone.0181851)
26. Haubrich C, Diehl RR, Kasprowicz M, Diedler J, Sorrentino E, Smielewski P, Czosnyka M. 2015 Traumatic brain injury: increasing ICP attenuates respiratory modulations of cerebral blood flow velocity. *Med. Eng. Phys.* **37**, 175–179. (doi:10.1016/j.medengphy.2014.11.009)
27. Santamarta D, Abásolo DE, Martínez-Madrigal M, Hornero R. 2012 Characterisation of the intracranial pressure waveform during infusion studies by means of central tendency measure. *Acta Neurochir.* **154**, 1595–1602. (doi:10.1007/s00701-012-1441-y)
28. Katzman R, Hussey F. 1970 A simple constant-infusion manometric test for measurement of CSF absorption. I. Rationale and method. *Neurology* **20**, 534–544.
29. Rioul O, Vetterli M. 1991 Wavelets and signal processing. *IEEE Signal Process. Mag.* **8**, 14–38. (doi:10.1109/79.91217)
30. Addison PS. 2017 *The illustrated wavelet transform handbook: introductory theory and applications in science, engineering, medicine and finance*, 2nd edn. Boca Raton, FL: CRC Press.
31. Torrence C, Compo GP. 1998 A practical guide to wavelet analysis. *Bull. Am. Meteorol. Soc.* **79**, 61–78. (doi:10.1175/1520-0477(1998)079<0061:APGTWA>2.0.CO;2)
32. Mallat S. 2008 *A wavelet tour of signal processing: the sparse way*. New York, NY: Academic Press.
33. Roach BJ, Mathalon DH. 2008 Event-related EEG time-frequency analysis: an overview of measures and an analysis of early gamma band phase locking in schizophrenia. *Schizophr. Bull.* **34**, 907–926. (doi:10.1093/schbul/sbn093)
34. Bachiller A, Poza J, Gómez C, Molina V, Suazo V, Hornero R. 2015 A comparative study of event-related coupling patterns during an auditory oddball task in schizophrenia. *J. Neural Eng.* **12**, 016007. (doi:10.1088/1741-2560/12/1/016007)
35. Poza J, Gómez C, García M, Corralejo R, Fernández A, Hornero R. 2014 Analysis of neural dynamics in mild cognitive impairment and Alzheimer's disease using wavelet turbulence. *J. Neural Eng.* **11**, 026010. (doi:10.1088/1741-2560/11/2/026010)
36. Turalska M, Latka M, Pierzchala K, West BJ, Czosnyka M. 2009 Generation of very low frequency cerebral blood flow fluctuations in humans. *Acta Neurochir. Suppl.* **102**, 43–47. (doi:10.1007/978-3-211-85578-2_9)
37. Poza J, Gómez C, García M, Bachiller A, Fernández A, Hornero R. 2014 Analysis of spontaneous MEG activity in mild cognitive impairment and Alzheimer's disease using Jensen's divergence. In *Proc. 36th Ann. Int. Conf. IEEE-EMBS, Chicago, IL, 23–30 August*, pp. 1501–1504. Piscataway, NJ: IEEE.
38. Kowalski AM, Martín MT, Plastino A, Rosso OA, Casas M. 2011 Distances in probability space and the statistical complexity setup. *Entropy* **13**, 1055–1075. (doi:10.3390/e13061055)
39. Lamberti PW, Majtey AP. 2003 Non-logarithmic Jensen–Shannon divergence. *Phys. A Stat. Mech. Appl.* **329**, 81–90. (doi:10.1016/S0378-4371(03)00566-1)
40. Poza J *et al.* 2017 Spatio-temporal fluctuations of neural dynamics in mild cognitive impairment and Alzheimer's disease. *Curr. Alzheimer Res.* **14**, 924–936. (doi:10.2174/1567205014666170309115656)
41. Jobson JD. 1991 *Applied multivariate data analysis*. New York, NY: Springer.
42. Stankovski T, Petkoski S, Raeder J, Smith AF, McClintock PVE, Stefanovska A. 2016 Alterations in the coupling functions between cortical and cardio-respiratory oscillations due to anaesthesia with propofol and sevoflurane. *Phil. Trans. R. Soc. A* **374**, 20150186. (doi:10.1098/rsta.2015.0186)
43. Silvani A, Calandra-Buonaura G, Dampney RAL, Cortelli P. 2016 Brain–heart interactions: physiology and clinical implications. *Phil. Trans. R. Soc. A* **374**, 20150181. (doi:10.1098/rsta.2015.0181)
44. Bateman GA. 2000 Vascular compliance in normal pressure hydrocephalus. *Am. J. Neuroradiol.* **21**, 1574–1585.
45. Bianciardi M, Toschi N, Polimeni JR, Evans KC, Bhat H, Keil B, Rosen BR, Boas DA, Wald LL. 2016 The pulsatility volume index: an indicator of cerebrovascular compliance based on fast magnetic resonance imaging of cardiac and respiratory pulsatility. *Phil. Trans. R. Soc. A* **374**, 20150184. (doi:10.1098/rsta.2015.0184)

46. Wagshul ME, Kelly EJ, Yu HJ, Garlick B, Zimmerman T, Egnor MR. 2009 Resonant and notch behavior in intracranial pressure dynamics. *J. Neurosurg. Pediatr.* **3**, 354–364. (doi:10.3171/2009.1.PEDS08109)
47. Haubrich C, Czosnyka ZH, Lavinio A, Smielewski P, Diehl RR, Pickard JD, Czosnyka M. 2007 Is there a direct link between cerebrovascular activity and cerebrospinal fluid pressure-volume compensation? *Stroke* **38**, 2677–2680. (doi:10.1161/STROKEAHA.107.485847)
48. Egnor MR, Zheng L, Rosiello A, Gutman F, Davis R. 2002 A model of pulsations in communicating hydrocephalus. *Pediatr. Neurosurg.* **36**, 281–303. (doi:10.1159/000063533)
49. Bateman GA, Levi CR, Schofield P, Wang Y, Lovett EC. 2008 The venous manifestations of pulse wave encephalopathy: windkessel dysfunction in normal aging and senile dementia. *Neuroradiology* **50**, 491–497. (doi:10.1007/s00234-008-0374-x)
50. Schmidt EA, Czosnyka ZH, Momjian S, Czosnyka M, Bech RA, Pickard JD. 2005 Intracranial baroreflex yielding an early Cushing response in human. *Acta Neurochir. Suppl.* **95**, 253–256. (doi:10.1007/3-211-32318-X-51)
51. Keissar K, Davrath LR, Akselrod S. 2009 Coherence analysis between respiration and heart rate variability using continuous wavelet transform. *Phil. Trans. R. Soc. A* **367**, 1393–1406. (doi:10.1098/rsta.2008.0273)
52. Hu X, Alwan AA, Rubinstein EH, Bergsneider M. 2006 Reduction of compartment compliance increases venous flow pulsatility and lowers apparent vascular compliance: implications for cerebral blood flow hemodynamics. *Med. Eng. Phys.* **28**, 304–314. (doi:10.1016/j.medengphy.2005.07.006)
53. Addison PS. 2015 A review of wavelet transform time-frequency methods for NIRS-based analysis of cerebral autoregulation. *IEEE Rev. Biomed. Eng.* **8**, 78–85. (doi:10.1109/RBME.2015.2436978)
54. Kasprowicz M, Asgari S, Bergsneider M, Czosnyka M, Hamilton R, Hu X. 2010 Pattern recognition of overnight intracranial pressure slow waves using morphological features of intracranial pressure pulse. *J. Neurosci. Methods* **190**, 310–318. (doi:10.1016/j.jneumeth.2010.05.015)